PCCP

PAPER

View Article Online
View Journal | View Issue



Cite this: *Phys. Chem. Chem. Phys.*, 2025, **27**, 23245

# Tuning linear dichroism/birefringence (LDLB) contributions in VCD spectra of tartaric acid-$TPPS_4$ porphyrin films

Giuseppe Mazzeo, [a] Marco Fusè, [a] Sergio Abbate, [ab] Roberto Zagami, [c] Maria Angela Castriciano, [c] Andrea Romeo, [c] Luigi Monsù Scolaro *[c] and Giovanna Longhi *[ab]

Received 11th August 2025,
Accepted 13th October 2025

DOI: 10.1039/d5cp03069b

rsc.li/pccp

Vibrational circular dichroism (VCD) is employed to investigate chiral-templation of D and L tartaric acids (TA) which, according to electronic circular dichroism (ECD) studies, drive tetrakis-(4-sulfonatophenyl)porphyrin ($TPPS_4$) to self-assemble into chiral J-aggregates. $TPPS_4$/TA solutions, prepared in both $H_2O$ and $D_2O$, are drop cast on $CaF_2$ plates. VCD spectra of corresponding films are not affected by rotating the samples around the incident beam, but undergo dramatic changes, even sign reversal, by flipping the samples from "front" to "rear" position, depending on acid content. The observed IR absorption features are mainly due to vibrational transitions of TA. The dissymmetry ratio g for the observed features is of the order of $10^{-2}$, which is quite high for vibrational phenomena: the semi-sum spectra in the front-rear positions can be considered as representative of "intrinsic" VCD phenomena, the semi-difference is associated with linear dichroism-linear birefringence components (LDLB term). In this study, we show that $TPPS_4$ and TA, when mixed appropriately following the specified protocols, yield films in which the VCD and LDLB components can be effectively modulated.



## Introduction

Vibrational circular dichroism (VCD) experiments are usually conducted on solutions mainly to assign the absolute configuration of chiral compounds (either of natural or synthetic origin),[1–4] to investigate conformational properties[5–7] of molecular or supramolecular systems[8,9] or secondary peptide structure.[10,11] VCD has been demonstrated to be a sensitive technique to conformational changes and environment interactions. Use of IR solid state spectroscopy has always been of primary interest, especially by employing KBr pellets.[12] Despite its 50 year history,[13] the use of VCD for solid state samples is not common[14,15] being prone to artifact. However, in recent years, both CD and VCD spectroscopies in solid state have met significant attention and are catching up rapidly both experimentally and theoretically.[16–21] Particular interest has emerged in the fields of material science[22,23] and quality control,[16,24,25] considering both pellets and films.[26,27] Recently, important advances in solid state VCD calculations have been developed.[28–30] The VCD spectrum of a compound in the solid state may be quite different from the one recorded in solution. In crystal form, molecules are packed in regular lattices and the conformational freedom is quite restricted leading to narrower IR and VCD bands.[29] Moreover, interactions with nearby molecules are stronger and can generate supramolecular chiral structures. As a result, solid state VCD can be rich in relevant information. However, it requires particularly careful experimental procedures in order to discriminate effects of different nature. The great interest in the subject is also witnessed by the recent publication of a review article titled "VCD beyond solutions".[31]

The various contributions affecting VCD in the solid state and its electronic counterpart (ECD), though to a different degree, have been discussed in the literature, where many papers have appeared. We cite here just a few of them, to the risk of being impolite to some Authors, all of them applying the Mueller matrix method,[13,26,27,32–38] and touching upon most aspects of optical activity of solid state samples, even VCD and films. Without entering in detailed explanations, here we just quickly recall the contributions to an observed spectrum of "so called CD": (1) circular dichroism, namely absorption difference of the two types of circularly polarized light (CD); (2) linear dichroism, namely absorption difference of the two linearly

[a] *Dipartimento di Medicina Molecolare e Traslazionale, Università di Brescia, Viale Europa, 11, 25123 Brescia, Italy. E-mail: giovanna.longhi@unibs.it*
[b] *Istituto Nazionale di Ottica CNR, Unità di Brescia, Via Branze 45, 25123 Brescia, Italy*
[c] *Dipartimento di Scienze Chimiche, Biologiche, Farmaceutiche ed Ambientali, Università di Messina, V. le F. Stagno D'Alcontres, 31, 98166 Messina, Italy. E-mail: luigi.monsuscolaro@unime.it*

polarized components at two orthogonal axes (LD and LD′ for two 45°-rotated axes pairs); (3) differences in the refraction indexes of the two circularly polarized components (CB = circular birefringence, otherwise called ORD = optical rotatory dispersion); (4) differences in the refraction indexes of the two linearly polarized components at two orthogonal axes (LB and LB′ = linear birefringence for two 45°-rotated axes pairs). We are mostly interested in the first contribution (CD) and even though LD and LB may be thought of as artifacts —or more precisely, as ''disturbances''—in CD studies, their contributions may be exploited for some applications.[39] Apart from distortions caused by crystal scattering (Christensen effect),[40] depending on the size of solid particles/aggregates, LD and LB receive contributions from intrinsic solid medium anisotropy (particles or films) due to linear alignment of organized structures within the sample, leading to significant differences in refraction indices (LB/CB) for orthogonal states or linear polarization.[13] Salji *et al.*[36] have recently proposed a semiclassical treatment to calculate LD/LB response.

Considering the VCD enhancement often observed in the solid state and the richness of signals typical of the IR spectroscopic range, the use of solid state VCD can be quite informative. In the present work, we aim to contribute to the use of VCD analysis for film characterization. To this instance we have undertaken the study of films obtained from the zwitterionic form $H_2TPPS_4$ of tetrakis-(4-sulfonatophenyl)porphyrin ($TPPS_4$) for which the group in Messina has long experience.[41–47] Acidic $TPPS_4$ are involved in an end-to-end self-association mechanism giving rise to aggregates in solution which exhibit an excitonically coupled spectrum corresponding to an intense UV absorption band at longer wavelength (at about 490 nm) with respect to the corresponding Soret monomer band, known as Jelley-Scheibe (J-band), accompanied by a less intense H-band at shorter wavelength (at about 420 nm).[48,49] J and H components (see Scheme 1) are both present due to the nanotube supramolecular structure, despite the fact that in the literature they are usually indicated as J-aggregates being their spectroscopic signature the one that dominates. Also Q bands, often disregarded being very weak, are indicative of J-aggregate presence, signaled by absorption at 706 nm and correspondingly CD activity (see Fig. S2 right panels). UV and ECD spectroscopies allow to monitor such J-aggregation condition in which the protonated positive core of one molecule has electrostatic interactions with negative sulfonate groups of adjacent molecules (see Scheme 1). We recall that porphyrins have been widely studied focusing on chirality transfer phenomena[50–53] also in aggregated form.[54–56]

An interesting property of $TPPS_4$ system is that it exhibits symmetry breaking phenomenon even in achiral conditions.[41,57,58] Acidic environment contributes to accelerating or controlling the aggregation kinetics and the counter-anions play an important role according to the Hofmeister series. Chiral self-assembling is sensitive to initial conditions such as pH, ionic strength and concentration.[42,44,59] To this instance, in the work by Occhiuto *et al.*[43] $TPPS_4$ micromolar solutions (3 μM) show an intense positive ECD couplet at 490 nm (+,− while decreasing wavelength), whose intensity is strongly dependent on the ability of counter-anions to interfere with hydrogen-bonding network of the solvent. In this work, we employed millimolar (1 mM) acid $TPPS_4$ solutions and obtained an opposite chiral behavior: a negative ECD couplet (Fig. S1) centered at 490 nm (however we reproduced the same results of ref.[41] when working at the same micro-molar concentration employed there). A further interesting feature of the formation of $TPPS_4$ aggregates, already pointed out by Zagami *et al.*,[60] is a kinetic effect experienced in $D_2O$ solutions which promote J-aggregation faster than in $H_2O$ solutions.

The mechanism of symmetry breaking in $TPPS_4$ system, in absence of chiral agents, is still under debate and is beyond the scope of this research; in this work, instead, we exploited $TPPS_4$ J-aggregates, chirally triggered by addition of solutions of D- and L-tartaric acid enantiomers (TA) whose formation in solution can be easily monitored by ECD-UV.[43]

Once aggregates are formed, as proven by absorption and ECD spectra (Fig. S2), we used such solutions to deposit drop-cast films on $CaF_2$ plates and we examined them through VCD. We report the crude experimental results for various film orientations and examine data taken first with the IR beam impinging directly on the film and afterwards data obtained with the light beam incident on the opposite, clean surface of the $CaF_2$ plate (flipped positions): we call the two positions ''front'' and ''rear'' respectively. Once acquired the data, orientation-averages and sum and difference spectra for the ''front'' and ''rear'' data are considered. Since observed IR bands are dominated by tartaric acid contributions, we examined also DMSO solutions, KBr-pellets and drop-cast film obtained by water TA solutions. Also, in this case solid state spectra are analyzed in terms of CD, LD and LB contributions.

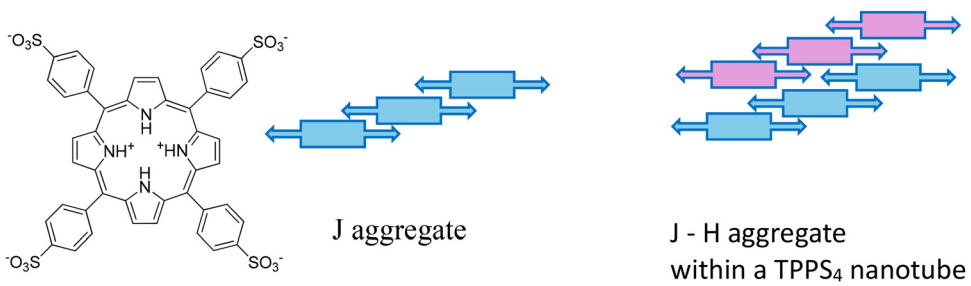


Scheme 1 Diacid form structure of $TPPPS_4$, schematics of J-aggregate scheme, and of J–H aggregation within a nanotube.

 

In fact, in this work it will be shown that linear dichroism-linear birefringence contributions, generally ascribed as ''side effects'', are quite reproducible; this point is rather important to apply computational models like those by Salji *et al.*[36] One of the main outcomes of the present analysis is that experimental conditions can be controlled in order to modulate all components to the overall CD spectra that is, ''true'' CD and LD-LB contributions.

## Results and discussion

### Treatment of solid state data

The original aim of this work was to study films obtained from chiral porphyrin J-aggregates *via* VCD-IR spectroscopy. First, we illustrate how we will analyze such data. Solid state crystalline and film analysis by VCD was first carried out by Buffeteau *et al.*,[26] Merten *et al.*,[27] Lombardi and Nafie,[35,61] Polavarapu[14] (as recently reviewed[31] by Krupová and Andrushchenko). These studies build upon the seminal work by Shindo and Nakagawa,[34] who utilized Mueller matrix analysis[62–64] mainly to investigate CD in the UV-vis range. This type of analysis allows to evaluate the linear contribution effects of the solid state within the observed CD spectral data ($CD_{obs}$), corresponding namely to the actual signal recorded by CD instrumentation. This means that the recorded spectra may be sensitive to rotation or flipping of the solid-state sample with respect to the direction of the light beam. In the following equation are indicated the various most important factors contributing to $CD_{obs}$ in the solid state:[26,27]

$$CD_{obs} \approx CD + \frac{1}{2}(LD' \cdot LB - LD \cdot LB') + \dots . \qquad (1)$$

where CD is the ''true CD'' (position-insensitive to sample rotation and flipping) and the second term relates to linear dichroism (LD/LD′) and linear birefringence (LB/LB′) taking place at different axes rotated by 45°, which will be here reported as LDLB. Terms averaging out upon rotation around the beam direction and higher order terms as discussed in ref. 65, are left out of eqn (1). A couple of comments are in order. First, as stated by Shindo[37] in a paper collecting his patient and constant work through the years and by Troxell and Scheraga *et al.*,[32] eqn (1) derives from a power series development of the Mueller matrix, with the first term being linear in film thickness and the second one being quadratic in film thickness. Parenthetically we wish to report that, in his work, Shindo recognized the great merit of Gō[38] in explaining and reviewing the Mueller matrix method. Secondly, one should include more contributions to eqn (1), as generated by instrumental artifacts, including, among others, static birefringence of photo-elastic modulator (PEM) and linear contributions that come from monochromators, photomultipliers, source, linear polarizer, *etc.*; such contributions generate spurious signals when the light interacts with samples showing LD and/or LB and can be partially compensated by rotating the solid sample along the light beam axis direction.[34,61]

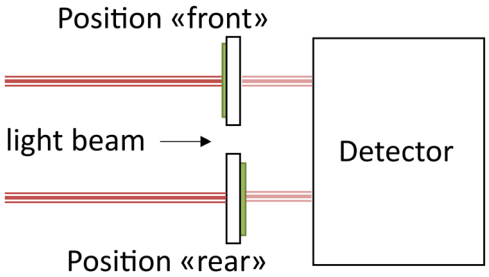


Scheme 2 Schematic representation and definition of the VCD/IR experiments on J-aggregates $TPPS_4$ films. Green layers depict the film layer and $CaF_2$ plate (in white) relative position.

The first and the second terms of (1) can be extracted as the semi-sum and semi-difference of front and rear obtained VCD observed spectra. Front and rear position are considered as reported in Scheme 2: we repeat here that front means that the film faces the incident light beam and rear the opposite position.[27,66] Starting from eqn (1) and according to considerations reported in ref. 27, it is possible to define the following quantities in eqn (2):

$$CD = \frac{1}{2}(CD_{front} + CD_{rear})$$
$$LDLB = \frac{1}{2}(LD'LB - LDLB') = \frac{1}{2}(CD_{front} - CD_{rear}) \qquad (2)$$

The previous analysis has received increasing attention in the recent literature: on one side a clearer rationalization has been reached, secondly applications are possible of what originally were thought artifacts to avoid. Starting from the study of chiroptical effects of plasmonic nanostructures[67] the concept of ''2D chirality'' has been introduced and adopted also for CD in the solid state. A 2D-chiral object presents two planar structures that cannot be brought one into the other whichever symmetry operation is performed within the plane. The CD inversion behavior due to ''2D chirality'' can be exploited in a Fabry–Pérot cavity to enhance the chiroptical signal.[68] By analyzing various examples of films presenting prevalent LDLB component, the presence of anisotropic birefringent domains has been evidenced.[69,70] Another component could be circular differential scattering associated to crystallization domains.[71]

### VCD of tartaric acid in different preparations

Since the main aim of the present study was to characterize with VCD chiral porphyrin aggregates templated by tartaric acid used in large molarity ratio with respect to $TPPS_4$ (see in the following) we preliminarily examined VCD spectra of tartaric acid (TA) *per se*, measured in different conditions, that is in DMSO solution and different solid-state preparations. As expected, data taken at solid state reveal an enhancement of VCD signals but also an important LDLB contribution to the overall spectra. We report in Fig. S3 VCD-IR spectra of TA in deuterated DMSO solution (data compare well with ref. 72) and as KBr pellets. We would like to recall that the first VCD

spectrum on TA was recorded by Sugeta *et al.*[73] in the CH stretching region, and recently Sato *et al.* measured VCD of TA in an organoclay nanohybrid with quantum cascade laser (QCL) setup.[74] In the past, IR spectra of KBr pellets as well as of films and melt tartaric acids had been studied, in optically active form, in meso-form and as racemates. The major differences were found in the OH-stretching region, while mid-IR seems less sensitive to the different preparation procedures.[73,75–77] Commenting VCD data (Fig. S3), we may notice a *ca.* three times intensification of the experimental g dissymmetry ratio from solution to KBr pellets. It is also important to report that KBr pellets did not provide any anisotropic effect and, consequently, no change of VCD spectra upon flipping or rotating pellets was observed. This is because of the efficacious grinding process of the solid compounds, thus ensuring homogeneous dispersion of the sample in the pellet.[19]

The large dissymmetry ratio represents an advantage in employing solid state measurements since shorter accumulation time is required with respect to solution measurements: on our apparatus, each solution measurement generally needs 6000 accumulations (about 1 hour) while KBr pellet measurements needed only 2000 accumulations to provide clear VCD spectra with acceptable signal to noise ratio.

We then drop-cast a tartaric acid film on $CaF_2$ plates starting from a 100 mM $H_2O$ solution. TA does not give rise to homogeneous films on the plates but it rather crystallizes in spots providing very clear and intense anisotropic ''front/rear'' features in observed VCD spectra which are one order of magnitude more intense than ''true CD'' contributions (Fig. S4). The fact that front and rear spectra of each enantiomer are nearly mirror image implies that the main contribution is from LDLB term: applying eqn (2) one obtains LDLB spectra with dissymmetry factor g *ca.* $10^{-1}$ ($10^{-3}$ for CD). It should be noted that in these latter conditions the measurements required only 50 accumulations (about 2 minutes) to provide reliable spectra. IR spectra (used together with VCD to evaluate *g*-factors) are independent on both the orientation of the film and also upon flipping from front to rear and, and they are nearly identical for the two enantiomers of TA.

### Preparation of $TPPS_4$/TA films and VCD analysis

After checking the high variability of TA VCD spectra in different physical states of the sample, we examined cast films obtained from $TPPS_4$/TA aggregates. In order to create the proper chiral environment which is able to enantiomerically drive $TPPS_4$ J-aggregation, 100 mM solutions of D/L-TA were added to a 1 mM porphyrin solution prepared according to a ''porphyrin first'' protocol.[41] In the first series of experiment we mixed the two solutions 6 : 4, *i.e.* 6 parts in volume of $TPPS_4$ solution to 4 parts of TA solution. Starting solutions were prepared using both $H_2O$ and $D_2O$ as solvent and we monitored the formation of both aggregates *via* ECD-UV spectroscopy (J-aggregates driven by D-TA and L-TA will be defined here as $J_D$ and $J_L$ respectively). Seven days old $J_D$ and $J_L$ solutions showed enantiomeric ECD couplets as reported in Fig. S2. As one can note, J-aggregation took place to a good degree, showing intense enantiomeric couplets centered at 490 nm while there is a decrease of the 434 nm UV band, this latter being allied to the $TPPS_4$ diprotonated monomeric form. The H aggregate component is difficult to identify within the absorption spectrum, since it appears as a shoulder only slightly blue-shifted with respect to the monomeric absorption band: however, the CD doublet centered at 420 nm can be considered as indicative of the presence of H-aggregate component. The two J and H aggregation mechanisms are present within the $TPPS_4$ nanotube as described in reference[78] Furthermore, we can notice an isotopic effect:[60] $D_2O$ gave one order of magnitude more intense ECD with respect to ordinary water (see also the UV spectra) after seven days. In $D_2O$ solutions, ECD bands related to Q bands are also detectable in the spectrum (Fig. S2, inset) not present in the $H_2O$ aggregates. This isotopic effect was already noted[60] and spectroscopically characterized for $TPPS_4$ aggregates formed in very diluted acidic solutions (about 3 μM) comparing DCl/$D_2O$ and HCl/$H_2O$ mixtures, identifying inverse kinetic and equilibrium isotope effects. In general, it is often the case that, due to the lower vibrational frequency and thus due to a lower zero point vibrational energy,[79] deuterium gives energetically more stable aggregates and has influence on the kinetics promoting a faster process and so ultimately controls nanostructure formation.[80]

For the VCD experiments, $J_D$ and $J_L$ drop-cast films on $CaF_2$ plates were prepared from the previously described solutions, after checking with ECD the proper aggregate formation, and both $H_2O$ and $D_2O$ preparations were used. 24 hours were enough to obtain films at 20 °C.

The VCD-IR spectra of the films actually showed only TA signals (due to larger amounts of TA with respect to $TPPS_4$ in the parent solutions).

All VCD spectra taken on $TPPS_4$/TA films are practically insensitive to plate rotation around the radiation beam (Fig. S5). LDLB contribution is large, as immediately suggested by the fact that the front and rear positions yield quite different recorded spectra (Fig. 1), though not with all features of opposite sign as those observed in pure TA films; in that case, the CD contribution was only a minimal part of the recorded signal.

Taking into account eqn (2), one can extract from the recorded spectra of Fig. 1 the CD and the LDLB contributions which we report in Fig. 2. It is worth noting that CD and LDLB spectra are characterized by absolute intensities of similar order of magnitude, which is indicative of the fact that the presence of porphyrin aggregates is more efficient in providing reliable CD data than simple TA drop-casting; in the latter case in fact anisotropic effects were at least one order of magnitude more intense than ''true'' CD (Fig. S4). One may also notice that both $H_2O$ and $D_2O$ films show nearly identical absorption spectra in the recorded spectroscopic region (see also ref. 77) (Fig. S6), and quite similar, albeit not identical, VCD spectra, (Fig. 2, upper panels), while LDLB spectra are more substantially different (Fig. 2, lower panels); this may suggest that the LDLB component is strictly tied to aggregate formation kinetics and their film deposition, while CD is less sensitive and more

 

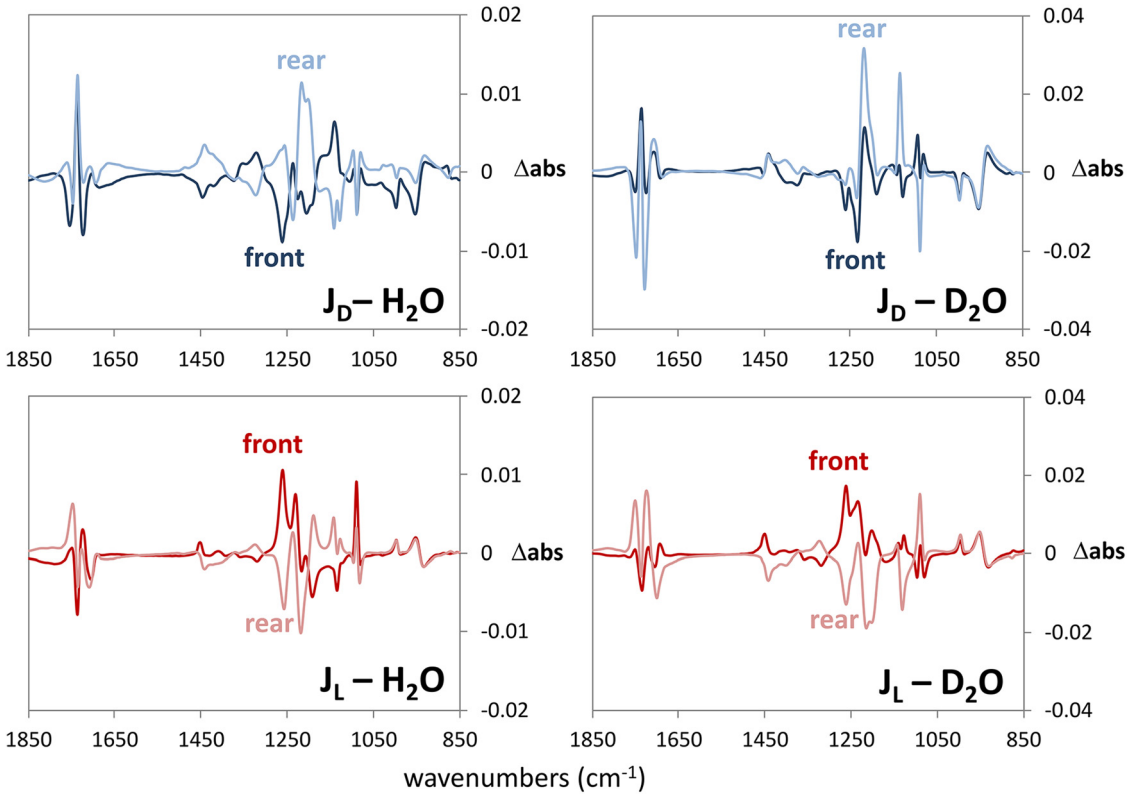


Fig. 1 VCD spectra comparison of front and rear (dark/light color traces respectively) position of films of $J_D$ (upper panels) and $J_L$ (lower panels) aggregates. Reported VCD spectra refer to $H_2O$ (left panels) and $D_2O$ (right panels) drop cast solutions on $CaF_2$ plates (see text). Experimental conditions: [$TPPS_4$] = 0.6 mM; [TA] = 40 mM (lower panel). Molar ratio [TA/$TPPS_4$] ≈ 67.

reproducible considering different preparation following the same protocol.

### Varying LDLB contribution

The obtained similarity of the VCD spectra for these films make us confident to consider such templation mechanism useful in handling anisotropic effects of the solid-state conditions in the recorded spectra. Such an approach was impossible to apply for the cast film of mere TA, where true CD contribution was too weak with respect to LDLB. This indeed means that by treating TA-porphyrin aggregates we got some control over the drop-casting procedure which is for sure straight, fairly quick and simple but not always exactly reproducible.[81] Once established the efficiency of $TPPS_4$ in promoting formation of regular films to obtain solid state VCD spectra, we changed $TPPS_4$ : TA mixture ratio from 6 : 4 to 8 : 2, *i.e.* we performed drop-casting of $J_D$ and $J_L$ aggregates by mixing 800 μL of $TPPS_4$ and 200 μL tartaric acid of previously described stock solutions (see Fig. S7), in this case the final concentration of acid is 25 times that of porphyrin. In Fig. S8 and S9 we report the comparison of true CD and LDLB VCD spectra, respectively, for both 6 : 4 and 8 : 2 $J_D$ and $J_L$ mixtures. Interestingly, one may notice that both VCD spectra and LDLB contributions, in the case of 8 : 2 films, appear to be more regular and enantiomeric with respect to the previous 6 : 4 case.

Coming now to an analysis of VCD spectra, we observe that the two sets of films show very similar features in the range 1100–1500 $cm^{-1}$ while, in the lower wavenumber region (850–1000 $cm^{-1}$), the triplets exhibited in 6 : 4 films (Fig. S8, upper panels) are not detected in the 8 : 2 ones. The 1650–1850 $cm^{-1}$ region with CO stretching features shows an overall similar trend, while relative intensities change when changing TA content or solvent ($H_2O$ *versus* $D_2O$). Analyzing the origin of these differences is not easy since the exact structures/conformations of the molecules within the film are not known. VCD is highly sensitive to molecular conformations which can be stabilized by differences in molecular packing that in turn depend on the $TPPS_4$ content, on the kinetics of aggregate formation in solution, and on the casting process.

As previously reported, acidic conditions promote J-aggregation.[43] For this reason we decided also to drop-cast films obtained from 8 : 2 ($TPPS_4$ : TA) $J_D$ and $J_L$ water solutions with further addition of HCl (20 μL 1 M HCl solution in 500 μL 8 : 2 J-aggregate solutions) in order to investigate whether the VCD spectra are affected by such conditions. The acidification effect was monitored by ECD-UV in which the increase of the aggregate 490 nm band with respect to the 434 nm of the monomeric form is quite evident (see Fig. S10). In this case, we still confirmed rotation-insensitive VCD spectra of $J_D$ and $J_L$ films but also absence of LDLB contributions. VCD spectra of front and rear orientations for both $J_D$ and $J_L$ samples are almost superimposable (see Fig. S11 upper panels) and comparison between data of films obtained from aggregates in HCl-acidified solutions and data of original 8 : 2 films shows very

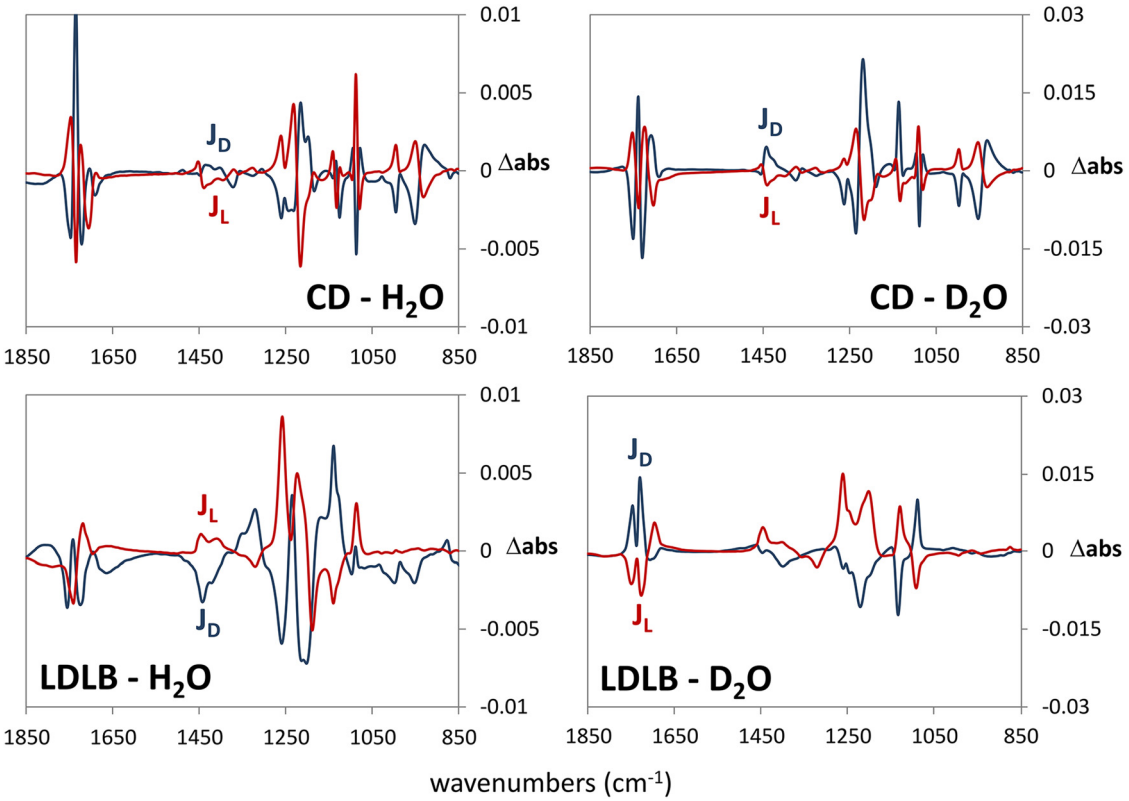


Fig. 2 Comparison of $J_D$ (blue lines) and $J_L$ (red lines) aggregate VCD spectra obtained by summing the recorded spectra of Fig. 1 (indicated as CD, upper panels) and of LDLB anisotropic contribution obtained by subtracting the data of Fig. 1 (lower panels). VCD spectra in the left panels refer to $H_2O$ and in the right panels to ($D_2O$ drop cast solutions on $CaF_2$ plates). Experimental conditions: [$TPPS_4$] = 0.6 mM; [TA] = 40 mM (lower panel). Molar ratio [TA/$TPPS_4$] $\approx$ 67.

similar features in the whole 850–1850 $cm^{-1}$ region (Fig. 3). $J_D$ and $J_L$ data appear almost enantiomeric confirming the ability of $TPPS_4$ to promote regular film templation, furthermore, this result suggests that the more the J-aggregation process is completed in solution the less the films are affected by anisotropic contribution. Since J-aggregates of $TPPS_4$ are formed by linear arrangements of porphyrins, often leading to well-structured nanotubes, the experimental evidence could be ascribed to the ability of such nanostructures of interacting and in some way controlling the TA environment during the formation of the films. This effect should be stronger in the presence of longer nanotubes or fibers. In fact, passing from less to more acidic conditions by addition of inorganic strong acid, J-aggregates are expected to grow longer as proved by the increase of the 490 nm band in the UV-Vis spectra.

Details about the structural aspects of the prepared films accounting for the different spectroscopic response deserve further future investigations, herein we just try to clarify the role played by TA, $TPPS_4$ and acid addition in the resulting spectroscopic behavior.

The highest LDLB content is undoubtedly observed for pure TA films and the reason for that and for the macroscopic inhomogeneity of the films is allied to its propensity to crystallize. TA acts as the chiral seed, initiating and guiding the emergence of chirality at increasing hierarchical levels, promoting chiral manifestations of all preparations. TA crystals are 3D-chiral superstructures: when observed in pellets, that is in isotropic medium, they give ''true'' CD (unless there is some preferred orientation induced during the preparation of the pellet, but that does not seem to be the case within the sensitivity limits of our instrumentation). When TA crystals grow on a window plate, they have an up and down direction and are no more isotropically distributed. Having an above-sided and a below-sided face, the resulting CD spectra are different when light impinges on either sides giving a very similar situation to what has been called in the recent literature ''2D-chirality''.[67,69,70] From Fig. S13a and S14a, one can observe that TA crystals organize in elongated structures covered by semi-amorphous material.

$TPPS_4$ nanotubes in solutions are 3D chiral superstructures with chirality induced by TA, and they are formed in an isotropic environment and are randomly oriented. As the solution dries, $TPPS_4$ aggregates impede or, better, limit and continue the extended formation of TA crystallites, that appear as isolated entities (see Fig. S13b, c and S14b, c); concurrently, $TPPS_4$ fibrils' spatial arrangement is influenced by TA crystallization nuclei. So, while the $TPPS_4$ nanotube component is organized in fibrils (see Fig. S13b, right panel) and is perturbed by TA crystallites, thus exhibiting high variability in its ECD response in the UV-VIS region, on the contrary, the same films

 

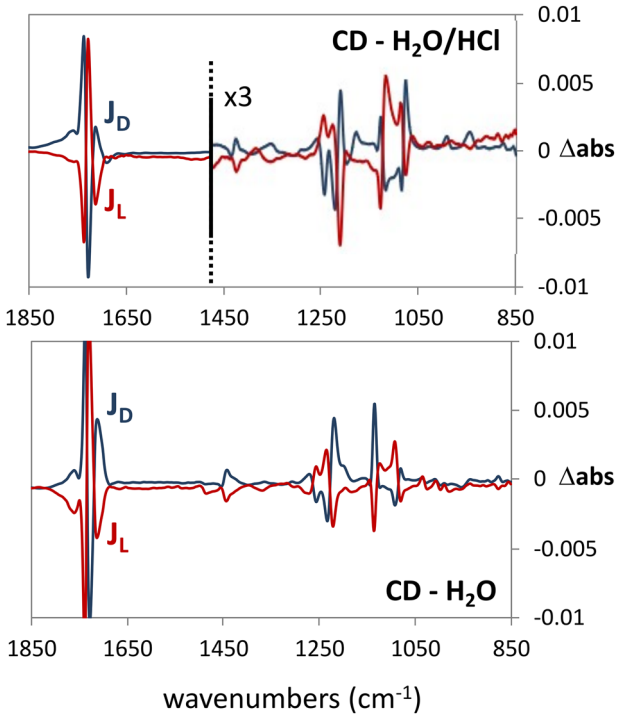


Fig. 3 Comparison between $J_D$ (blue lines) and $J_L$ (red lines) aggregate VCD spectra as obtained by summing the originally recorded spectra on drop cast film from $H_2O$/HCl solution: [$TPPS_4$] = 0.77 mM; [TA] = 19.2 mM; [HCl] = 38.5 mM (upper panel) and $H_2O$ solution: [$TPPS_4$] = 0.8 mM; [TA] = 20 mM (lower panel) (Molar ratio [TA/$TPPS_4$] ≈ 25).

yield highly reproducible results when analyzed by VCD spectroscopy, which selectively probes the randomly distributed TA crystallites: LDLB spectral contribution, in fact, is indicative of a residual crystallization. In any case, "true" VCD can be clearly disentangled from the front and rear recorded spectra, the lower the TA:$TPPS_4$ ratio the better (see Fig. S7).

The results obtained upon addition of HCl to the $TPPS_4$/TA water solution confirm the above description, assuming that HCl modifies TA crystallization: in this last case, in fact, not only VCD spectra are invariant upon flipping (no detectable LDLB component), but also UV-VIS ECD spectra, where $TPPS_4$ absorbs, are reproducible and do not show sensible changes upon flipping (Fig. S11 and S12). From Fig. S13d and S14d one can see that samples rearrange in a different fashion: crystals are still present but showing a microcrystalline dendritic or fractal structure.

All the above considerations indicate that TA crystallization nuclei are responsible of the LDLB component at VCD and also of perturbing the $TPPS_4$ nanotube arrangement.

## Conclusions

In this work, we have made use of diacid $TPPS_4$, which is easily driven to form chiral J-aggregates whose handedness is determined by templation with either D or L enantiomers of TA: aggregation in $H_2O$ and $D_2O$ solutions can be easily monitored by ECD-UV technique. Once aggregation in solution is established, films are deposited by drop-casting on $CaF_2$ plates. The VCD-IR technique confirms that the combination $TPPS_4$/TA promotes the formation of uniform, reproducible films leading to consistent optical properties across multiple samples. It is also shown that chiroptical properties of such films can be tuned upon changing the relative molar ratio of the porphyrin system and of TA or upon acidification and even by considering $D_2O$ instead of $H_2O$ starting solutions. While "true" VCD main features (invariant upon flipping the depositing $CaF_2$ plate from front to rear orientation) are common to different film preparations, linear dichroism-linear birefringence components (LDLB term) seem strictly connected to aggregate formation kinetics and to film deposition. All film measurements showed a dissymmetry factor of $10^{-2}$, which is quite high with respect to common dissymmetry factor registered in the IR range.

The fact that the $TPPS_4$ peculiar properties permit to strongly influence and direct the aggregation and subsequent film formation process such as to have some control over the resulting drop-cast films, is indeed important in view of the growing interest towards optically active films employed as optoelectronic layers or for tuning absorption/emission of circularly polarized light or for sensing and many other applications. In this context VCD spectroscopy reveals to be an important tool to characterize aggregation states in films at multiple hierarchical levels, testing the quality of chiral supramolecular solid-state arrangement.

Regarding the two actors of this study, this investigation provides useful addition to the studies of TA in the solid state, which have a long history in chirality, ranging from the seminal separation of TA enantiomers *via* crystallization à-la-Pasteur[82] to one of the first determination *via* X-ray diffraction[83] to neutron-scattering studies[84] and recent co-crystallization studies.[85–87] Regarding porphyrin and chiral supramolecular structures thereof, we recall their recent use for basic studies of phenomena like MCD and magnetochiral dichroism (MChD),[54,55] for the development of good substrates to evidence Chiral Induced Spin Selectivity (CISS) effect[88,89] and for application as sensor of chiral excess in inorganics[90] or vapor enantiomers recognition[91] just to cite some examples.

## Materials and methods

Tetrakis-(4-sulfonatophenyl)porphyrin ($TPPS_4$) and tartaric acid (TA, D and L) solutions were obtained by dissolving the solids in $H_2O$ and $D_2O$ to 1 mM and 100 mM concentrations respectively. $J_D$ and $J_L$ aggregates were obtained by adding TA solutions in the $TPPS_4$ porphyrin solution in either 4 : 6 or 2 : 8 ratio. The further acidification procedure consisted in adding 20 μL of a 1 M HCl solution to 500 μL J-aggregates mixtures.

$J_D$ and $J_L$ films were obtained by drop cast depositing 60 μL of TA/$TPPS_4$ mixtures on 13 mm-diameter $CaF_2$ plates and letting the solvent to evaporate for 12 hours.

VCD/IR measurements were carried out using a Jasco FVS 6000 apparatus equipped with a ZnSe photo-elastic modulator

(PEM), working at 50 kHz frequency modulation, placed past a wire grid linear polarizer and synchronously gauged to a lock-in amplifier. An MCT liquid-$N_2$ cooled diode-detector for the regions 850–2000 $cm^{-1}$ was employed. VCD spectra of films were recorded by rotating the sample in 90°-steps around the light beam axis and by also flipping the samples. All solid state VCD spectra are reported as average over the spectra of the four rotated films. 6000 scans were acquired for DMSO-$d_6$ measurement and solvent spectra were taken in the same conditions and subtracted out. 2000 scans were acquired for KBr pellets TA and 50 accumulations for films measurements. Resolution was set at 4 $cm^{-1}$. ECD/UV measurements were conducted with Jasco 815SE with 0.1 mm quartz cell in $H_2O$ and $D_2O$ solutions. ECD/UV measurements have also been conducted on the same film deposited on $CaF_2$ plates.

For microscopy investigations 20 μL of the solutions containing TA, or the TA/$TPPS_4$ mixtures were deposited by drop cast onto commercial 4-inch silicon wafer 100-orientation, 500 μm thickness, n-type 1–5 Ohm $cm^{-1}$ of resistivity (Siegert Wafer). Scanning Electron Microscopy (SEM) images were acquired by using a Zeiss Gemini 460 by using an InLENS detector and 10 kV of extraction voltage.

Digital Microscope images were obtained by using a Keyence VHX7000 in backscattering and dark field conditions.

## Author contributions

All authors have contributed to the final version of the manuscript.

## Conflicts of interest

There are no conflicts to declare.

## Data availability

All experimental procedures and characterization data are available in the supplementary information (SI). Supplementary information: ECD spectra of $TPPS_4$ + tartaric acid systems in $H_2O$ and $D_2O$ solutions. IR and VCD spectra of tartaric acid enantiomers in KBr pellets and DMSO solution and as films prepared by evaporating the solvent. VCD spectra of $TPPS_4$ + tartaric acid systems prepared from $H_2O$ and $D_2O$ solutions in various orientation and conditions. ECD spectra of $TPPS_4$ + tartaric acid systems with addition of a small HCl quantity. SEM and optical images of the TA and $TPPS_4$ + tartaric acid systems. See DOI: **https://doi.org/10.1039/d5cp03069b**.

## Acknowledgements

Funding by the Italian Ministry of University and Research (MUR): projects SMART HELIX, prot. 2022B3EFJH, INVESTCPE, prot. 2022CXHY3A, CHI-EP (PRIN_2022HPW79T_002) and Next Generation EU, PNRR Samothrace Project (ECS00000022) is acknowledged. The authors acknowledges also the Italian Project PNNR "I-PHOQS—Integrated Infrastructure Initiative in Photonic and Quantum Science" CUP B53C22001750006 and Prof. Antonio Leonardi for SEM and optical microscopy. The authors wish to thank the reviewers, who provided insightful suggestions for improving the manuscript and for pointing out relevant literature.

## References

1 G. Mazzeo, A. Cimmino, M. Masi, G. Longhi, L. Maddau, M. Memo, A. Evidente and S. Abbate, Importance and Difficulties in the Use of Chiroptical Methods to Assign the Absolute Configuration of Natural Products: The Case of Phytotoxic Pyrones and Furanones Produced by Diplodia Corticola, *J. Nat. Prod.*, 2017, **80**(9), 2406–2415, DOI: **10.1021/acs.jnatprod.7b00119**.

2 P. L. Polavarapu, *Chiroptical Spectroscopy: Fundamentals and Applications*, CRC Press, Boca Raton, 2016, DOI: **10.1201/9781315374888**.

3 M. Fusè, G. Mazzeo, G. Longhi, S. Abbate, M. Masi, A. Evidente, C. Puzzarini and V. Barone, Unbiased Determination of Absolute Configurations by Vis-à-Vis Comparison of Experimental and Simulated Spectra: The Challenging Case of Diplopyrone, *J. Phys. Chem. B*, 2019, **123**(43), 9230–9237, DOI: **10.1021/acs.jpcb.9b08375**.

4 M. Ravutsov, G. M. Dobrikov, M. Dangalov, R. Nikolova, V. Dimitrov, G. Mazzeo, G. Longhi, S. Abbate, L. Paoloni, M. Fusè and V. Barone, 1,2-Disubstituted Planar Chiral Ferrocene Derivatives from Sulfonamide-Directed Ortho-Lithiation: Synthesis, Absolute Configuration, and Chiroptical Properties, *Organometallics*, 2021, **40**(5), 578–590, DOI: **10.1021/acs.organomet.0c00712**.

5 G. Longhi, S. Ghidinelli, S. Abbate, G. Mazzeo, M. Fusè, S. E. Boiadjiev and D. A. Lightner, Insights into the Structures of Bilirubin and Biliverdin from Vibrational and Electronic Circular Dichroism: History and Perspectives, *Molecules*, 2023, **28**(6), 2564, DOI: **10.3390/molecules28062564**.

6 C. Merten, F. Li, K. Bravo-Rodriguez, E. Sanchez-Garcia, Y. Xu and W. Sander, Solvent-Induced Conformational Changes in Cyclic Peptides: A Vibrational Circular Dichroism Study, *Phys. Chem. Chem. Phys.*, 2014, **16**(12), 5627–5633, DOI: **10.1039/C3CP55018D**.

7 S. Ma, S. Shen, H. Lee, N. Yee, C. Senanayake, L. A. Nafie and N. Grinberg, Vibrational Circular Dichroism of Amylose Carbamate: Structure and Solvent-Induced Conformational Changes, *Tetrahedron: Asymmetry*, 2008, **19**(18), 2111–2114, DOI: **10.1016/j.tetasy.2008.08.027**.

8 C. Bravin, G. Mazzeo, S. Abbate, G. Licini, G. Longhi and C. Zonta, Helicity Control of a Perfluorinated Carbon Chain within a Chiral Supramolecular Cage Monitored by VCD, *Chem. Commun.*, 2022, **58**(13), 2152–2155, DOI: **10.1039/D1CC06861J**.

9 C. Müller, K. Scholten, E. Engelage and C. Merten, Synthesis and VCD Spectroscopic Characterization of a Series of Azacryptands from a Chiral Valine-Based Derivative of

Tris(2-Aminoethyl)Amine (TREN), *Chem. – Eur. J.*, 2023, **29**(63), e202302126, DOI: 10.1002/chem.202302126.
10 P. L. Polavarapu and Ch Zhao, Vibrational Circular Dichroism: A New Spectroscopic Tool for Biomolecular Structural Determination, *Fresenius' J. Anal. Chem.*, 2000, **366**(6), 727–734, DOI: 10.1007/s002160051566.
11 T. A. Keiderling, Structure of Condensed Phase Peptides: Insights from Vibrational Circular Dichroism and Raman Optical Activity Techniques, *Chem. Rev.*, 2020, **120**(7), 3381–3419, DOI: 10.1021/acs.chemrev.9b00636.
12 L. J. Bellamy, *The Infra-Red Spectra of Complex Molecules*, Wiley, London, Chapman and Hall, New York, 1975.
13 L. A. Nafie, *Vibrational Optical Activity: Principles and Applications*, Wiley, Chichester, West Sussex, 2011.
14 P. Zhang and P. L. Polavarapu, Vibrational Circular Dichroism of Matrix-Assisted Amino Acid Films in the Mid-Infrared Region, *Appl. Spectrosc.*, 2006, **60**(4), 378–385, DOI: 10.1366/000370206776593807.
15 H. Sato, I. Kawamura, A. Yamagishi and F. Sato, Solid-State Vibrational Circular Dichroism Spectra of Isoleucine and Its Related Compounds: Effects of Interplay between Two Chiral Centers, *Chem. Lett.*, 2017, **46**(4), 449–452, DOI: 10.1246/cl.161043.
16 K. Dobšíková, T. Taušová, P. Fagan, N. Paškanová, M. Kuchař, J. Čejka and V. Setnička, Solid-State Vibrational Circular Dichroism: Methodology and Application for Amphetamine Derivatives, *Spectrochim. Acta, Part A*, 2024, **305**, 123486, DOI: 10.1016/j.saa.2023.123486.
17 H. Sato and I. Kawamura, Solid-State Vibrational Circular Dichroism Studies on the Conformation of an Amino Acid Molecule in Crystalline State, *Biochim. Biophys. Acta, Protein Struct.*, 2020, **1868**(8), 140439, DOI: 10.1016/j.bbapap.2020.140439.
18 J. E. Rode, K. Łyczko, D. Kaczorek, R. Kawęcki and J. Cz Dobrowolski, VCD Spectra of Chiral Naphthalene-1-Carboxamides in the Solid-State, *Spectrochim. Acta, Part A*, 2024, **310**, 123939, DOI: 10.1016/j.saa.2024.123939.
19 E. Castiglioni, P. Biscarini and S. Abbate, Experimental Aspects of Solid State Circular Dichroism, *Chirality*, 2009, **21**(1E), E28–E36, DOI: 10.1002/chir.20770.
20 M. Caricato, A Perspective on the Simulation of Electronic Circular Dichroism and Circularly Polarized Luminescence Spectra in Chiral Solid Materials, *J. Phys. Chem. A*, 2024, **128**(7), 1197–1206, DOI: 10.1021/acs.jpca.3c08095.
21 H. Sato, S. Inoué, J. Yoshida, I. Kawamura, J. Koshoubu and A. Yamagishi, Microscopic Vibrational Circular Dichroism on the Forewings of a European Hornet: Heterogenous Sequences of Protein Domains with Different Secondary Structures, *Phys. Chem. Chem. Phys.*, 2024, **26**(25), 17918–17922, DOI: 10.1039/D4CP01827C.
22 H. Sato, K. Takimoto, A. Yamagishi, J. Yoshida and M. Hara, Vibrational Circular Dichroism Spectroscopy toward Intercalation Compounds of Sodium Montmorillonite: Evidences for Molecular Packing of Enantiopure Monovalent Ir(III) Complexes within Interlayer Spaces, *Appl. Clay Sci.*, 2022, **228**, 106621, DOI: 10.1016/j.clay.2022.106621.
23 S. Aisawa, N. Horiguchi, C. Chida, J. Sang, H. Hirahara, A. Yamagishi and H. Sato, Nanoscale Chirality Generated in Zinc(II) Orthophosphate Clusters: Evidence by Vibrational Circular Dichroism, *Nanoscale*, 2024, **16**(44), 20589–20595, DOI: 10.1039/D4NR03809F.
24 L. A. Nafie and R. K. Dukor, Pharamaceutical Applications of Vibrational Optical Activity, in *Applications of Vibrational Spectroscopy in Pharmaceutical Research and Development*, ed. D. Pivonka, P. R. Griffiths and J. M. Chalmers, John Wiley & Sons, Ltd., Chichester, West Sussex, United Kingdom, 2007, pp. 129–154.
25 H. Sato, S. Aisawa, H. Ida, M. Shimizu, K. Watanabe, J. Koshoubu, J. Yoshida and I. Kawamura, Two-Dimensional Imaging of a Model Pharmaceutical Dosage Tablet Using a Scanning Vibrational Circular Dichroism System, *Chem. Lett.*, 2022, **51**(2), 205–207, DOI: 10.1246/cl.210635.
26 T. Buffeteau, F. Lagugné-Labarthet and C. Sourisseau, Vibrational Circular Dichroism in General Anisotropic Thin Solid Films: Measurement and Theoretical Approach, *Appl. Spectrosc.*, 2005, **59**(6), 732–745, DOI: 10.1366/0003702054280568.
27 C. Merten, T. Kowalik and A. Hartwig, Vibrational Circular Dichroism Spectroscopy of Solid Polymer Films: Effects of Sample Orientation, *Appl. Spectrosc.*, 2008, **62**(8), 901–905, DOI: 10.1366/000370208785284394.
28 J. E. Rode, K. Lyczko, K. Kosińska, J. Matalińska, J. Dyniewicz, A. Misicka, J. Cz Dobrowolski and P. F. J. Lipiński, The Solid State VCD of a Novel N-Acylhydrazone Trifluoroacetate, *Spectrochim. Acta, Part A*, 2022, **269**, 120761, DOI: 10.1016/j.saa.2021.120761.
29 S. Jähnigen, Vibrational Circular Dichroism Spectroscopy of Chiral Molecular Crystals: Insights from Theory, *Angew. Chem., Int. Ed.*, 2023, **62**(41), e202303595, DOI: 10.1002/anie.202303595.
30 S. Jähnigen, R. Vuilleumier and A. Zehnacker, The Genesis of OH-Stretching Vibrational Circular Dichroism in Chiral Molecular Crystals, *Chem. Sci.*, 2025, **16**(22), 9833–9842, DOI: 10.1039/D4SC08055F.
31 M. Krupová and V. Andrushchenko, Vibrational Circular Dichroism beyond Solutions, *Spectrochim. Acta, Part A*, 2025, **340**, 125839, DOI: 10.1016/j.saa.2025.125839.
32 T. C. Troxell and H. A. Scheraga, Electric Dichroism and Polymer Conformation. I. Theory of Optical Properties of Anisotropic Media, and Method of Measurement, *Macromolecules*, 1971, **4**(5), 519–527, DOI: 10.1021/ma60023a001.
33 Y. Shindo and Y. Ohmi, Problems of CD Spectrometers. 3. Critical Comments on Liquid Crystal Induced Circular Dichroism, *J. Am. Chem. Soc.*, 1985, **107**(1), 91–97, DOI: 10.1021/ja00287a017.
34 Y. Shindo and M. Nakagawa, On the Artifacts in Circularly Polarized Emission Spectroscopy, *Appl. Spectrosc.*, 1985, **39**(1), 32–38, DOI: 10.1366/0003702854249358.
35 R. A. Lombardi and L. A. Nafie, Observation and Calculation of Vibrational Circular Birefringence: A New Form of Vibrational Optical Activity, *Chirality*, 2009, **21**(1E), E277–E286, DOI: 10.1002/chir.20816.
36 A. Salij, R. H. Goldsmith and R. Tempelaar, Theory of Apparent Circular Dichroism Reveals the Origin of Inverted

and Noninverted Chiroptical Response under Sample Flipping, *J. Am. Chem. Soc.*, 2021, **143**(51), 21519–21531, DOI: 10.1021/jacs.1c06752.

37 Y. Shindo, Application of Polarized Modulation Technique in Polymer Science, *Opt. Eng.*, 1995, **34**(12), 3369–3384, DOI: 10.1117/12.213252.

38 N. Go, Optical Activity of Anisotropic Solutions. II, *J. Phys. Soc. Jpn.*, 1967, **23**, 88–97, DOI: 10.1143/JPSJ.23.88.

39 M. Liu, E. Plum, H. Li, S. Duan, S. Li, Q. Xu, X. Zhang, C. Zhang, C. Zou, B. Jin, J. Han and W. Zhang, Switchable Chiral Mirrors, *Adv. Opt. Mater.*, 2020, **8**(15), 2000247, DOI: 10.1002/adom.202000247.

40 G. Laufer, J. T. Huneke, B. S. H. Royce and Y. C. Teng, Elimination of Dispersion-induced Distortion in Infrared Absorption Spectra by Use of Photoacoustic Spectroscopy, *Appl. Phys. Lett.*, 1980, **37**(6), 517–519, DOI: 10.1063/1.91996.

41 R. Zagami, M. A. Castriciano, A. Romeo and L. M. Scolaro, Kinetic Investigations on the Chiral Induction by Amino Acids in Porphyrin J-Aggregates, *Int. J. Mol. Sci.*, 2023, **24**(2), 1695, DOI: 10.3390/ijms24021695.

42 M. A. Castriciano, A. Romeo, V. Villari, N. Micali and L. M. Scolaro, Structural Rearrangements in 5,10,15,20-Tetrakis(4-Sulfonatophenyl)Porphyrin J-Aggregates under Strongly Acidic Conditions, *J. Phys. Chem. B*, 2003, **107**(34), 8765–8771, DOI: 10.1021/jp0273880.

43 I. G. Occhiuto, R. Zagami, M. Trapani, L. Bolzonello, A. Romeo, M. A. Castriciano, E. Collini and L. M. Scolaro, The Role of Counter-Anions in the Kinetics and Chirality of Porphyrin J-Aggregates, *Chem. Commun.*, 2016, **52**(77), 11520–11523, DOI: 10.1039/C6CC05768C.

44 N. Micali, V. Villari, M. A. Castriciano, A. Romeo and L. Monsù Scolaro, From Fractal to Nanorod Porphyrin J-Aggregates. Concentration-Induced Tuning of the Aggregate Size, *J. Phys. Chem. B*, 2006, **110**(16), 8289–8295, DOI: 10.1021/jp060730e.

45 I. G. Occhiuto, M. A. Castriciano, M. Trapani, R. Zagami, A. Romeo, R. F. Pasternack and L. Monsù Scolaro, Controlling J-Aggregates Formation and Chirality Induction through Demetallation of a Zinc(II) Water Soluble Porphyrin, *Int. J. Mol. Sci.*, 2020, **21**(11), 4001, DOI: 10.3390/ijms21114001.

46 M. A. Castriciano, A. Romeo, R. Zagami, N. Micali and L. M. Scolaro, Kinetic Effects of Tartaric Acid on the Growth of Chiral J-Aggregates of Tetrakis(4-Sulfonatophenyl)Porphyrin, *Chem. Commun.*, 2012, **48**(40), 4872–4874, DOI: 10.1039/C2CC00028H.

47 R. Zagami, M. A. Castriciano, A. Romeo, M. Trapani, R. Pedicini and L. Monsù Scolaro, Tuning Supramolecular Chirality in Nano and Mesoscopic Porphyrin J-Aggregates, *Dyes Pigm.*, 2017, **142**, 255–261, DOI: 10.1016/j.dyepig.2017.03.047.

48 O. Ohno, Y. Kaizu and H. Kobayashi, J-aggregate Formation of a Water-soluble Porphyrin in Acidic Aqueous Media, *J. Chem. Phys.*, 1993, **99**(5), 4128–4139, DOI: 10.1063/1.466109.

49 E. E. Jelley, Spectral Absorption and Fluorescence of Dyes in the Molecular State, *Nature*, 1936, **138**(3502), 1009–1010, DOI: 10.1038/1381009a0.

50 A. G. Petrovic, G. Vantomme, Y. L. Negrón-Abril, E. Lubian, G. Saielli, I. Menegazzo, R. Cordero, G. Proni, K. Nakanishi, T. Carofiglio and N. Berova, Bulky Melamine-Based Zn-Porphyrin Tweezer as a CD Probe of Molecular Chirality, *Chirality*, 2011, **23**(9), 808–819, DOI: 10.1002/chir.21001.

51 R. Randazzo, M. Gaeta, C. M. A. Gangemi, M. E. Fragalà, R. Purrello and A. D'Urso, Chiral Recognition of L- and D-Amino Acid by Porphyrin Supramolecular Aggregates, *Molecules*, 2019, **24**(1), 84, DOI: 10.3390/molecules24010084.

52 T. Hu, T. Liu, Z. Zhang, Y. Wang, Y. Yang, D. J. Young, C. Hu and J.-P. Lang, Precise Control of Chirality Transfer by Adjusting the Alkyl Substituents of Guests, *Dyes Pigm.*, 2019, **160**, 692–699, DOI: 10.1016/j.dyepig.2018.09.004.

53 L. Zhang, T. Wang, J. Jiang and M. Liu, Chiral Porphyrin Assemblies, *Aggregate*, 2023, **4**(1), e198, DOI: 10.1002/agt2.198.

54 G. Duroux, L. Robin, P. Liu, E. Dols, M. D. S. L. Mendes, S. Buffière, E. Pardieu, A. Scalabre, T. Buffeteau, S. Nlate, R. Oda, M. S. Raju, M. Atzori, C. Train, G. L. J. A. Rikken, P. Rosa, E. A. Hillard and E. Pouget, Induced Circular Dichroism from Helicoidal Nano Substrates to Porphyrins: The Role of Chiral Self-Assembly, *Nanoscale*, 2023, **15**(28), 12095–12104, DOI: 10.1039/D3NR02670A.

55 Y. Mulyana and K. Ishii, A Novel Aspect of Spectroscopy for Porphyrinic Compounds under Magnetic Fields, *Dalton Trans.*, 2014, **43**(47), 17596–17605, DOI: 10.1039/C4DT01428F.

56 R. van der Weegen, A. J. P. Teunissen and E. W. Meijer, Directing the Self-Assembly Behaviour of Porphyrin-Based Supramolecular Systems, *Chem. – Eur. J.*, 2017, **23**(15), 3773–3783, DOI: 10.1002/chem.201605872.

57 G. Schifino, M. Fortino, L. M. Scolaro and A. Pietropaolo, Chiral Self-Organization of the TPPS4 Porphyrin Assisted by Molecular Rotations, *Mol. Syst. Des. Eng.*, 2023, **8**(12), 1512–1519, DOI: 10.1039/D3ME00072A.

58 J. Sun, Y. Li, F. Yan, C. Liu, Y. Sang, F. Tian, Q. Feng, P. Duan, L. Zhang, X. Shi, B. Ding and M. Liu, Control over the Emerging Chirality in Supramolecular Gels and Solutions by Chiral Microvortices in Milliseconds, *Nat. Commun.*, 2018, **9**(1), 2599, DOI: 10.1038/s41467-018-05017-7.

59 N. Micali, F. Mallamace, A. Romeo, R. Purrello and L. Monsù Scolaro, Mesoscopic Structure of Meso-Tetrakis(4-Sulfonatophenyl)Porphine J-Aggregates, *J. Phys. Chem. B*, 2000, **104**(25), 5897–5904, DOI: 10.1021/jp991909a.

60 R. Zagami, A. Romeo, M. A. Castriciano and L. Monsù Scolaro, Inverse Kinetic and Equilibrium Isotope Effects on Self-Assembly and Supramolecular Chirality of Porphyrin J-Aggregates, *Chem. – Eur. J.*, 2017, **23**(1), 70–74, DOI: 10.1002/chem.201604675.

61 L. N. Nafie Vibrational Optical Activity: Principles and Applications, Wiley. Wiley.com. https://www.wiley.com/en-us/Vibrational+Optical+Activity%3A+Principles+and+Applications-p-9780470032480 (accessed 2023-03-15).

62 J. Schellman and H. P. Jensen, Optical Spectroscopy of Oriented Molecules, *Chem. Rev.*, 1987, **87**(6), 1359–1399, DOI: 10.1021/cr00082a004.

63 H. P. Jensen, J. A. Schellman and T. Troxell, Modulation Techniques in Polarization Spectroscopy, *Appl. Spectrosc.*, 1978, **32**(2), 192–200, DOI: **10.1366/000370278774331567**.

64 A. Schönhofer, H.-G. Kuball and C. Puebla, Optical Activity of Oriented Molecules. IX. Phenomenological Mueller Matrix Description of Thick Samples and of Optical Elements, *Chem. Phys.*, 1983, **76**(3), 453–467, DOI: **10.1016/0301-0104(83)85227-6**.

65 T. J. Ugras, Y. Yao and R. D. Robinson, Can We Still Measure Circular Dichroism with Circular Dichroism Spectrometers: The Dangers of Anisotropic Artifacts, *Chirality*, 2023, **35**(11), 846–855, DOI: **10.1002/chir.23597**.

66 G. Albano, G. Pescitelli and L. Di Bari, Reciprocal and Non-Reciprocal Chiroptical Features in Thin Films of Organic Dyes, *ChemNanoMat*, 2022, **8**(8), e202200219, DOI: **10.1002/cnma.202200219**.

67 O. Arteaga, J. Sancho-Parramon, S. Nichols, B. M. Maoz, A. Canillas, S. Bosch, G. Markovich and B. Kahr, Relation between 2D/3D Chirality and the Appearance of Chiroptical Effects in Real Nanostructures, *Opt. Express*, 2016, **24**(3), 2242, DOI: **10.1364/OE.24.002242**.

68 Z. Wang, C. Lin, K. Murata, A. S. A. Kamal, B. Lin, M. Chen, S. Tang, Y. Ho, C. Chen, C. Chen, H. Daiguji, K. Ishii and J. Delaunay, Chiroptical Response Inversion and Enhancement of Room-Temperature Exciton-Polaritons Using 2D Chirality in Perovskites, *Adv. Mater.*, 2023, **35**(42), 2303203, DOI: **10.1002/adma.202303203**.

69 G. Albano, M. Lissia, G. Pescitelli, L. A. Aronica and L. Di Bari, Chiroptical Response Inversion upon Sample Flipping in Thin Films of a Chiral Benzo[1,2-*b*:4,5-*b*′]Dithiophene-Based Oligothiophene, *Mater. Chem. Front.*, 2017, **1**(10), 2047–2056, DOI: **10.1039/C7QM00233E**.

70 G. Albano, M. Bertuolo, F. Zinna, A. Taddeucci, T. Jávorfi, R. Hussain, G. M. Farinola, G. Pescitelli, A. Punzi, G. Siligardi and L. Di Bari, Unravelling the Origin of Strong Non-Reciprocal Chiroptical Features in Thin Films of a Chiral Diketopyrrolo[3,4-*c*]Pyrrole Dye, *Nanoscale*, 2025, **17**(9), 5128–5140, DOI: **10.1039/D4NR04956J**.

71 A. von Weber, D. C. Hooper, M. Jakob, V. K. Valev, A. Kartouzian and U. Heiz, Circular Dichroism and Isotropy – Polarity Reversal of Ellipticity in Molecular Films of 1,1′-Bi-2-Naphtol, *ChemPhysChem*, 2019, **20**(1), 62–69, DOI: **10.1002/cphc.201800950**.

72 P. L. Polavarapu, C. S. Ewig and T. Chandramouly, Conformations of Tartaric Acid and Its Esters, *J. Am. Chem. Soc.*, 1987, **109**(24), 7382–7386, DOI: **10.1021/ja00258a022**.

73 H. Sugeta, C. Marcott, T. R. Faulkner, J. Overend and A. Moscowitz, Infrared Circular Dichroism Associated with the C–H Strecthing Vibration of Tartaric Acid, *Chem. Phys. Lett.*, 1976, **40**(3), 397–398, DOI: **10.1016/0009-2614(76)85104-4**.

74 S. Aisawa, C. Chida, H. Ida, J. Sang, H. Hirahara and H. Sato, Synthesis of Phenylalanine and Tartaric Acid Intercalated Layered Double Hydroxide (LDH): Investigation of Two Kinds of Chiral Molecules Interaction in Interlayer Space of LDH Using Solid-State Vibrational Circular Dichroism, *Appl. Clay Sci.*, 2023, **244**, 107108, DOI: **10.1016/j.clay.2023.107108**.

75 M. Charbonnier and C. Courty, Sur le spectre d'absorption infrarouge des acides tartriques, *J. Phys.*, 1967, **28**(7), 534–538, DOI: **10.1051/jphys:01967002807053401**.

76 L. I. Kozhevina, L. G. Skryabina and Yu. K. Tselinskii, The Interpretation of the Infrared Spectrum of Tartaric Acid, *J. Appl. Spectrosc.*, 1980, **33**(6), 1347–1351, DOI: **10.1007/BF00614043**.

77 R. Bhattacharjee, Y. S. Jain and H. D. Bist, Laser Raman and Infrared Spectra of Tartaric Acid Crystals, *J. Raman Spectrosc.*, 1989, **20**(2), 91–97, DOI: **10.1002/jrs.1250200206**.

78 Z. El-Hachemi, C. Escudero, F. Acosta-Reyes, M. T. Casas, V. Altoe, S. Aloni, G. Oncins, A. Sorrenti, J. Crusats, J. L. Campos and J. M. Ribó, Structure *vs.* Properties—Chirality, Optics and Shapes—in Amphiphilic Porphyrin J-Aggregates, *J. Mater. Chem. C*, 2013, **1**(20), 3337, DOI: **10.1039/c3tc30299g**.

79 A. Kjaersgaard, E. Vogt, N. F. Christensen and H. G. Kjaergaard, Attenuated Deuterium Stabilization of Hydrogen-Bound Complexes at Room Temperature, *J. Phys. Chem. A*, 2020, **124**(9), 1763–1774, DOI: **10.1021/acs.jpca.9b11762**.

80 S. Du, Y. Jiang, H. Jiang, L. Zhang and M. Liu, Pathway-Dependent Self-Assembly for Control over Helical Nanostructures and Topochemical Photopolymerization, *Angew. Chem., Int. Ed.*, 2024, **63**(6), e202316863, DOI: **10.1002/anie.202316863**.

81 A. Kaliyaraj Selva Kumar, Y. Zhang, D. Li and R. G. Compton, A Mini-Review: How Reliable Is the Drop Casting Technique?, *Electrochem. Commun.*, 2020, **121**, 106867, DOI: **10.1016/j.elecom.2020.106867**.

82 L. Pasteur, Mémoires sur la relation qui peut exister entre la forme cristalline et la composition chimique et sur la cause de la polarisation rotatoire, *Compt. Rend.*, 1848, **26**, 535.

83 W. T. Astbury and W. H. Bragg, The Crystalline Structure and Properties of Tartaric Acid, *Proc. R. Soc. Lond. Ser. A Contain. Pap. Math. Phys. Character*, 1997, **102**(718), 506–528, DOI: **10.1098/rspa.1923.0010**.

84 Y. Okaya, N. R. Stemple and M. I. Kay, Refinement of the Structure of D-Tartaric Acid by X-Ray and Neutron Diffraction, *Acta Crystallogr.*, 1966, **21**(2), 237–243, DOI: **10.1107/S0365110X66002664**.

85 L. Roca-Paixão, N. T. Correia, F. Danède, M. Guerain and F. Affouard, Carbamazepine/Tartaric Acid Cocrystalline Forms: When Stoichiometry and Synthesis Method Matter, *Cryst. Growth Des.*, 2023, **23**(3), 1255–1369, DOI: **10.1021/acs.cgd.2c00859**.

86 A. Sarkar and S. Rohani, Cocrystals of Acyclovir with Promising Physicochemical Properties, *J. Pharm. Sci.*, 2015, **104**(101), 98–105, DOI: **10.1002/jps.24248**.

87 R. G. Kostyanovsky, V. R. Kostyanovsky and G. K. Kadorkina, The Enigma of a (±)-Tartaric Acid–Urea Cocrystal, *Mendeleev Commun.*, 2009, **19**(1), 17–18, DOI: **10.1016/j.mencom.2009.01.007**.

88 W. Mtangi, F. Tassinari, K. Vankayala, A. Vargas Jentzsch, B. Adelizzi, A. R. A. Palmans, C. Fontanesi, E. W. Meijer and R. Naaman, Control of Electrons' Spin Eliminates Hydrogen

Peroxide Formation During Water Splitting, *J. Am. Chem. Soc.*, 2017, **139**(7), 2794–2798, DOI: **10.1021/jacs.6b12971**.

89 C. Kulkarni, A. K. Mondal, T. K. Das, G. Grinbom, F. Tassinari, M. F. J. Mabesoone, E. W. Meijer and R. Naaman, Highly Efficient and Tunable Filtering of Electrons' Spin by Supramolecular Chirality of Nanofiber-Based Materials, *Adv. Mater.*, 2020, **32**(7), 1904965, DOI: **10.1002/adma.201904965**.

90 M. De Souza Lima Mendes, G. Duroux, A. Boudier, P. Pranee, Y. Okazaki, T. Buffeteau, S. Massip, S. Nlate, R. Oda, E. Hillard and E. Pouget, Porphyrin J-Aggregates as a Probe for Chiral Impurities as Demonstrated by Their Symmetry Breaking by Confinement in Montmorillonite Clay, *Nanoscale*, 2025, **17**(3), 1334–1341, DOI: **10.1039/D4NR03728F**.

91 I. Di Filippo, Z. Anfar, G. Magna, P. Pranee, D. Monti, M. Stefanelli, R. Oda, C. Di Natale and R. Paolesse, Chiral Porphyrin-$SiO_2$ Nano Helices-Based Sensors for Vapor Enantiomers Recognition, *Nanoscale Adv.*, 2024, **6**(17), 4470–4478, DOI: **10.1039/D4NA00217B**.

 